Demonstration of high-dimensional free-space data coding/decoding through multi-ring optical vortices

Shiyao Fu (付时尧)[1,2,3], Yanwang Zhai (翟焱望)[1,3], Heng Zhou (周 恒)[1,3], Jianqiang Zhang (张建强)[1,3], Ci Yin (殷 慈)[1,3], and Chunqing Gao (高春清)[1,3,*]

[1]*School of Optics and Photonics, Beijing Institute of Technology, Beijing 100081, China*
[2]*Institute of Advanced Structure Technology, Beijing Institute of Technology, Beijing 100081, China*
[3]*Key Laboratory of Photoelectronic Imaging Technology and System, Ministry of Education, Beijing 100081, China*
**Corresponding author: gao@bit.edu.cn*

Received March 19, 2019; accepted May 6, 2019; posted online July 9, 2019

Multi-ring optical vortices are a kind of structured beams that carry orbital angular momentum (OAM) and have concentrical doughnut intensity distributions. In this Letter, we present both theoretically and experimentally a scheme that employs the dimensions of both the OAM states and radial index of multi-ring optical vortices simultaneously to accomplish high-dimensional free-space data coding/decoding transmissions. Such a scheme can further improve the coding efficiency when limited OAM states are available. In the proof-of-concept experiment, 64-ary coding/decoding employing 16 OAM states and four radial indices are present. Also, the coding/decoding performance when facing various atmosphere turbulences is evaluated. Furthermore, a 64×64 gray image (totally, 32,768 bits) is also transmitted through multi-ring optical vortices coding in free-space successfully, showing good transmission performance.

OCIS codes: 060.2605, 050.4865, 050.1950.
doi: 10.3788/COL201917.080602.

Since Allen *et al.* proved that optical vortices with a helical wavefront carry orbital angular momentum (OAM) 26 years ago[1,2], such vortices have attracted more and more attention and found applications in lots of domains[3–14]. The complex amplitude of an optical vortex comprises the helical term $\exp(il\varphi)$, with l as the topological charge and φ as the azimuthal angle. The topological charge l, also known as OAM states, is the eigenvalue. Each photon in the optical vortices carries OAM $l\hbar$ ($\hbar$ is the Planck constant divided by 2π). Moreover, l can be an infinite integer in theory, and optical vortices with various l are mutually orthogonal. Hence, these features provide a new dimension, the OAM-based mode-division multiplexing (MDM), in classical optical communications, thus to further enlarge the capacity[3–6]. Meanwhile, such MDMs can be done simultaneously with the common wavelength-division multiplexing and polarization-division multiplexing, where hundred-terabit-scale data transmission can be accomplished[7]. Nevertheless, there is still controversy about OAM-based MDM, as some other limitations will also confine the transmission capacities. Thus, the capacities will not be increased infinitely[8,9].

In addition to MDM, the OAMs of optical vortices can also act as a data coding/decoding symbol, where N OAM states can represent $\log_2 N$ bits information. The OAM states corresponding to the value l are theoretically infinite, indicating that the OAM of optical vortices can carry an unlimited number of bits. Such features make it feasible to realize high-dimensional coding/decoding for free-space optical communication through employing multiple possible OAM states of vortices[4,10,15,16].

However, confines are still present for OAM-based data coding/decoding systems. One major limitation is that, although the OAM state l is infinite in theory, the available OAM states are limited in practice, where generating optical vortices with large l is difficult. What is worse, the needed OAM states will increase exponentially when more bits are encoded. Besides, for the decoding in the receiver side, large-tuning-range detecting of OAM states is also relatively difficult to realize. Therefore, a laudable way is to encode more information with fewer OAM states. Researchers have recently reported that multiple OAM arrays are employed to encode information, where the space dimension is introduced[17]. The encoding efficiency is improved compared with single OAM encoding. Nevertheless, we still need to find a convenient way to encode more information through one beam.

In this Letter, we demonstrate high-dimensional free-space data coding/decoding through multi-ring optical vortices for short-distance and large transmission capacity density scenarios as optical interconnects, optical networks, and so on. Different from the common single-ring vortices, multi-ring vortices have another dimension, the radial index, which contributes to many applications. For instance, the radial degree of freedom will benefit the optical information protocols from a quantum point of view[18–20]. Here, we show that such dimensions can also be employed for free-space data coding/decoding, which can be accomplished simultaneously with that of OAM. Indeed, generating multi-ring vortices and detecting the topological charge and radial index simultaneously are relatively complex compared with the common single-ring vortices, and multi-ring vortices have larger divergence

angles under same conditions, leading to a larger receiving aperture. However, the introduction of a radial index can further improve the coding efficiency when limited OAM states are available, which is positive for future optical communications. In the proof-of-concept experiment, 64-ary high-dimensional data multi-ring coding/decoding employing 16 OAM states and four radial indices, where each symbol carries 6 bits of information, is present. Based on the proposed high-dimensional multi-ring coding/decoding, a 64×64 gray image (32,768 bits in total) is transmitted in free-space with zero bit-error-rate (BER), showing good data transmission performance. Additionally, due to the fact that the outside atmosphere turbulence will distort the helical wavefront[21,22], we also evaluate the multi-ring coding/decoding performance when facing turbulence.

Multi-ring optical vortices have a multi-ring-shaped intensity distribution with concentric circles[1] and can be employed in multi-ring coding/decoding. The complex amplitude of multi-ring vortex beam reads as

$$|p, l\rangle \propto L_p^{|l|}\left(\frac{2r^2}{\omega^2}\right)\exp(il\varphi), \tag{1}$$

where p and l are the radial index and OAM state separately. (r, φ) is the radial and azimuthal coordinate, ω is the waist size, and $L_p^{|l|}(\zeta)$ is the associated Laguerre polynomial. The multi-ring structure mainly results from the radial-related associated Laguerre polynomial, where the number of the ring is $(p+1)$. When $p=0$, $L_p^{|l|}(\zeta)=1$; Eq. (1) represents the common single-ring optical vortices.

The concept and principle of high-dimensional multi-ring coding/decoding are sketched in Fig. 1. The whole system consists of two main parts. One is the transmitter, and the other is the receiver. In the transmitter, a sequence of N-ary numbers is coded into a sequence of time-varying multi-ring optical vortices in free-space to represent N different symbols, where each number can find its corresponding multi-ring optical vortices pattern as one-to-one mapping:

$$\begin{bmatrix} |p_1, l_1\rangle & |p_1, l_2\rangle & \cdots & |p_1, l_{N_l}\rangle \\ |p_2, l_1\rangle & |p_2, l_2\rangle & \cdots & |p_2, l_{N_l}\rangle \\ \vdots & \vdots & & \vdots \\ |p_{N_p}, l_1\rangle & |p_{N_p}, l_2\rangle & \cdots & |p_{N_p}, l_{N_l}\rangle \end{bmatrix}$$
$$\rightarrow \begin{bmatrix} 0 & 1 & \cdots & N_l-1 \\ N_l & N_l+1 & \cdots & 2N_l-1 \\ \vdots & \vdots & & \vdots \\ (N_p-1)N_l & (N_p-1)N_l+1 & \cdots & N_pN_l-1 \end{bmatrix}, \tag{2}$$

with N_l and N_p as the number of the utilized OAM states and radial indices, respectively, satisfying $N = N_l N_p$. During coding, numerous multi-ring vortices need to be generated to represent N symbols. In the past years, lots of approaches have been developed[23–25]. Here, holograms designed according to Ref. [23] are employed to generate optical vortices with various N_l OAM states and N_p radial indices. One can find easily that each symbol carries $\log_2 N_l$ bits information before introducing the radial index dimension, while such information increases to $\log_2 N = \log_2 N_l + \log_2 N_p$ bits with the radial index dimension. Hence, the information carried by each symbol increases $\log_2 N_p$ bits, indicating that multi-ring coding/decoding can further improve the coding efficiency when the available OAM states are fixed.

In the receiver, the transmitted multi-ring optical vortices sequence is captured and decoded into a sequence of N-ary numbers to recover the information. The decoding is done by a single hologram, the Dammann vortex grating[26,27], along with image processing. The Dammann vortex grating is a 0-π binary phase diffractive element, which can produce multiple optical vortices in various diffraction orders with different OAM states but equal intensities, also known as a vortices array, in the far field when Gaussian beams are incident. Similarly, once multi-ring optical vortices $|p, l\rangle$ propagate through a Dammann vortex grating, the far field diffractions are still a vortices array but with OAM states shifting. Supposing that the OAM states in diffraction order b are l_b when Gaussian beams are incident, such OAM state shifting in order b reads as

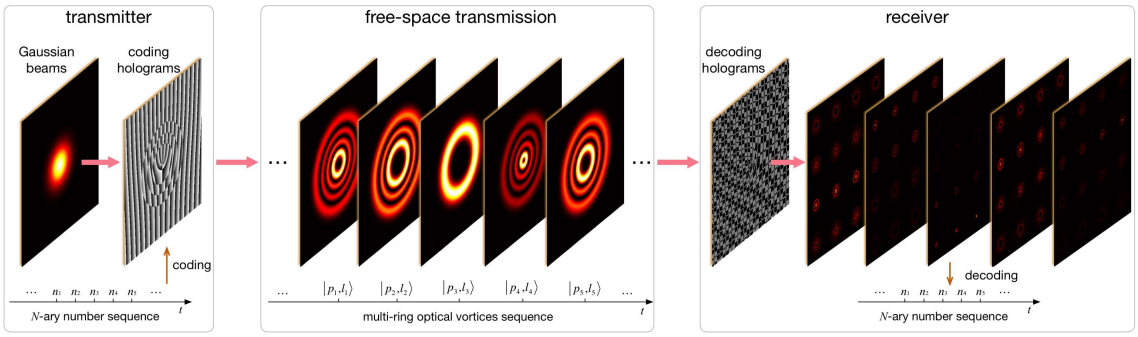

Fig. 1. Concept of high-dimensional multi-ring optical vortices coding/decoding.

$$|p, l\rangle \cdot \exp(il_b\varphi) = |p, l + l_b\rangle. \quad (3)$$

Once $l_b = -l$, the right side of Eq. (3) turns to be $|p, 0\rangle$, implying that the OAM is annihilated, and a bright spot will emerge in the beam center. Otherwise, the doughnut structure is still present, and the beam center is dark. Thus, the OAM state can be obtained. As for the radial index, the helical term $\exp(il_b\varphi)$ in Eq. (3) does not change in the radial dimension. Hence, one can gain the radial index from $|p, 0\rangle$, which is counting the number of its concentric circles.

By now, how to automatically determine the values p and l, which is extremely important for high-speed communications, must be addressed. Before the data transmission, we capture the decoding patterns for each N-ary symbol under back-to-back firstly. Then, we save them in the database as the original intensity matrix demarcates. When doing the data transmission, each captured decoded pattern is compared with the demarcated one to find the one with the highest correlation coefficient. Thus, l and p are determined, and the receiver can determine the represented N-ary number according to Eq. (2). Finally, the multi-ring optical vortices sequence is decoded into a sequence of N-ary numbers to recover the transmitted information.

Figure 2 gives the experimental setup. Fundamental Gaussian beams with the wavelength of 1.6 μm are produced by a distributed feedback laser and coupled into free-space. The polarized beam splitter (PBS) is placed to generate horizontally linear polarization, so as to meet the demand of phase only modulation of the following liquid-crystal spatial light modulator (SLM) (Holoeye, PLUTO-TELCO-013-C, nominal resolution 1920×1080 pixels, pixel pitch 8.0 μm). SLM1 is used to generate multi-ring optical vortices with various OAM states and radial indices for data coding. To achieve such a goal, each N-ary number corresponds to its specific coding hologram. When the N-ary number sequence changes over time, the hologram on SLM1 keeps switching and transforms the number sequence into a multi-ring optical vortices sequence in the first diffraction order, which is then filtered by a $4f$

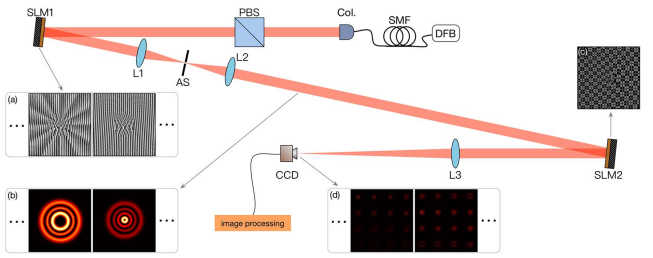

Fig. 2. Experimental setup. DFB, distributed feedback laser; SMF, single mode fiber; Col., collimator; PBS, polarized beam splitter; SLM1 and SLM2, liquid-crystal spatial light modulator; L1–L3, lenses; AS, aperture stop; CCD, infrared CCD camera. (a) The coding hologram sequence uploaded on SLM1. (b) The coded multi-ring optical vortices sequence. (c) The decoding hologram. (d) The decoded patterns.

system (lenses L1 and L2) along with an aperture stop. After propagating in free-space (2 m here), such a multi-ring optical vortices sequence is incident in SLM2, which is uploaded by a Dammann vortex grating. An infrared CCD camera is located at the image focal plane of L3 to capture the far field diffraction pattern. Such patterns are then analyzed by image processing, whose output is the recovered N-ary numbers. At that time, the decoding is accomplished.

The 6 bits high-dimensional multi-ring coding and decoding are carried out firstly in the experiment, where 16 various OAM states ($l \in [-9, -6] \cup [-4, -1] \cup [1, 4] \cup [6, 9] \cap \mathbb{Z}$) and four various radial indices ($p \in [0, 3] \cap \mathbb{Z}$) are employed to represent 64-ary numbers. In the transmitter, 64 different coding holograms designed according to the method given by Ref. [23] are uploaded on SLM1 to generate the above 64 multi-ring optical vortices, as shown in Fig. 3. One can find that each 64-ary number has its own corresponding multi-ring optical vortex. In the receiver, the Dammann vortex grating shown in Fig. 4(a) that can produce a 4×4 vortices array with the OAM states distribution of $l \in [-9, -6] \cup [-4, -1] \cup [1, 4] \cup [6, 9] \cap \mathbb{Z}$ is uploaded on SLM2. When the coded multi-ring vortices are incident in SLM2, a far-field decoding pattern, which is also a 4×4 vortices array, is captured by the CCD. Figure 4(b) gives the experimentally obtained decoding patterns for some of the symbols. One can find an apparent bright spot present at the desired location [the dashed circle marked in Fig. 4(b)], indicating the OAM state. Meanwhile, the radial index can be gained from the number of the concentric circles. After image processing through the previously mentioned decoding algorithm, the represented 64-ary number of each symbol is determined in a timely manner.

To further evaluate the performance of the proposed multi-ring optical-vortices-based high-dimensional data coding/decoding system, we transmit 5000 random 64-ary multi-ring vortices symbols (64-ary numbers), totally 30 kilobits information. After decoding, the received symbols are well recovered without seeing any error symbols, indicating that the proposed system has good data transmission performance.

One inevitable issue in practice is the atmosphere turbulence in the air. Such turbulence will distort the helical wavefront of optical vortices, broaden the OAM spectrum[21,22], and thus induce problems when decoding. Therefore, on the basis of the earlier 6 bits coding/decoding experiment, an additional experiment is done to evaluate the data transmission performance of the proposed system when facing turbulence. Here, the Fried parameter r_0 is used to represent the turbulence strength[28]. To simulate various atmosphere turbulences, turbulence phase masks based on the Kolmogorov turbulence model[29] are generated and combined together with the coding holograms. Once such holograms are loaded on SLM1, the data coding and atmospheric turbulence are introduced simultaneously. In this experiment, we transmit 300 random 64-ary numbers, totally 1.8 kilobits information, through 6 bits multi-ring coding/decoding. Their

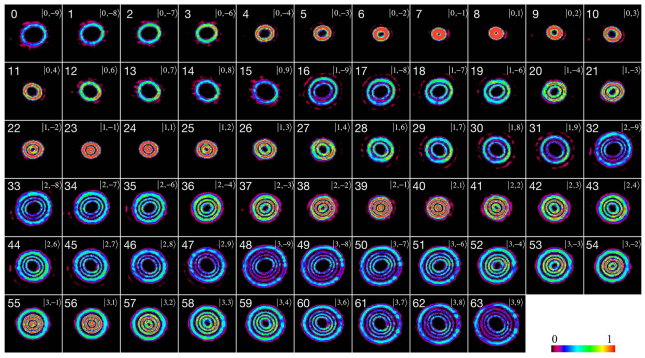

Fig. 3. Experimentally obtained 6 bits high-dimensional multi-ring coding for 64-ary numbers through 16 various OAM states and four various radial indices.

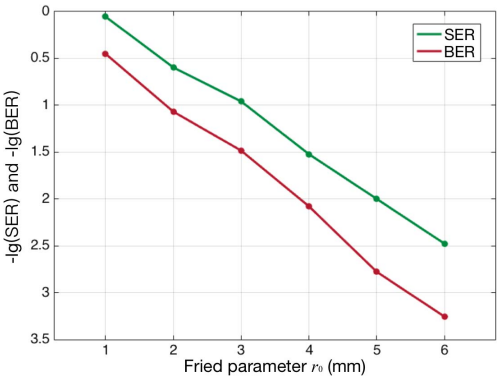

Fig. 5. Measured SER and BER versus Fried parameter r_0 for the proposed multi-ring vortices-based 6 bits coding/decoding system.

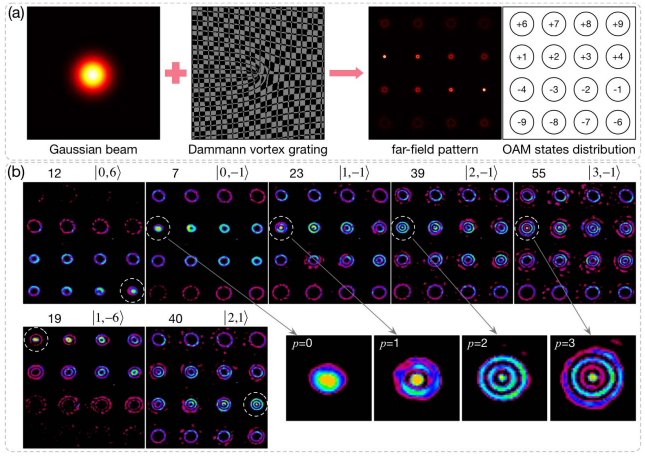

Fig. 4. (a) Dammann vortex grating employed in the experiment to produce 4×4 vortices array in the far field. (b) The captured decoding patterns for some of the symbols (7, 12, 19, 23, 39, 40, 55). The OAM states and radial indices are determined by the locations of the center bright spot and the number of concentric circles, respectively.

coding holograms are combined with a series of randomly produced, but r_0 fixed, turbulence phase masks to emulate time-varying atmospheric turbulence. In the receiver, the transmitted distorted symbols are analyzed, where the symbol-error-rate (SER) and BER are computed, as sketched in Fig. 5. From Fig. 5, one can find obviously that the measured SER and BER values decrease with the increasing of Fried parameter r_0, and the BER value will be lower than 1×10^{-3} when r_0 reaches 6 mm. Additionally, the measured BER value is smaller than the corresponding SER value for each r_0, as some bits existing with an error symbol might be correct. The phenomena shown in Fig. 5 imply that atmosphere turbulence will increase the BER and thus degrade the data transmission performance of a multi-ring vortices-based high-dimensional coding/decoding system.

Moreover, to show the data transmission performance of the proposed coding/decoding system vividly, a 64×64 gray image (the badge of Beijing Institute of Technology) shown in Fig. 6(a) with 256 gray-scale levels is transmitted in free-space. Each pixel of the gray image carries information of 8 bits, indicating such an image is 32,768 bits in total. Here, we also use 16 various OAM states ($l \in [-9,-6] \cup [-4,-1] \cup [1,4] \cup [6,9] \cap \mathbb{Z}$) and four various radial indices ($p \in [0,3] \cap \mathbb{Z}$) to represent 64-ary numbers, and thus to do the 6 bits coding/decoding. The symbol length is 5464 after coding, which is reduced by 5.997 times compared to that of the classic binary symbols, and by 1.499 times compared to that of single-ring optical vortices symbols under the same condition (only 16 various OAM states are used to represent the 4 bits symbol). When no turbulences are introduced, the transmitted gray image can be well recovered with 0 BER after decoding, as shown in Fig. 6(b). However, for the cases of turbulence $r_0 = 3$ mm and $r_0 = 1$ mm, noises emerge, as shown in Figs. 6(c) and 6(d), respectively. Specially, when $r_0 = 1$ mm, the recovered image is totally chaotic. The BER values for $r_0 = 3$ mm and $r_0 = 1$ mm are measured as 0.011 and 0.217, respectively. Figure 6 implies that atmosphere turbulence will degrade the data transmission performance, where approaches of turbulence compensation, as given in Refs. [30–33], must be introduced to correct such distortion.

It should be noticed the BER values for $r_0 = 3$ mm and $r_0 = 1$ mm in the results of Fig. 6 are different with those corresponding BER values in Fig. 5 that

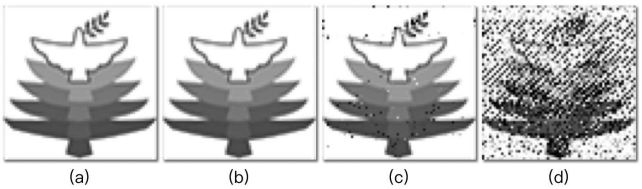

Fig. 6. Experimental results of transmitting a 64×64 gray badge of Beijing Institute of Technology through 6 bits multi-ring vortices coding/decoding with or without atmosphere turbulence. (a) The transmitted image. (b) The recovered image without turbulence. (c) The recovered image with turbulence $r_0 = 3$ mm. (d) The recovered image with turbulence $r_0 = 1$ mm.

are around 0.031 and 0.33. Such difference under the same turbulence strength is mainly the results from the randomness and dynamics of the turbulence mask. Here, the turbulence mask is generated through the Kolmogorov model, where a random complex matrix is introduced. Hence, under the same strength, various turbulence phase distributions will be present and finally lead to such a discrepancy.

The speed of data acquisition and the decoding process is extremely important for high-speed communications. The increased radial dimensions will cost more decoding time compared with classical OAM coding to some extent, which is not desirable for high-speed communications. Here, the decoding is done by the image processing program developed by our group, where the processing speed is associated with the hardware configuration of the computer. The time for processing each decoding pattern in the present work is about 0.1 s and is not fast enough. However, we are convinced that the decoding speed will further improve with the rapid development of computer hardware.

In summary, we have demonstrated a high-dimensional data coding/decoding system based on multi-ring optical vortices. We show that dimensions of the radial index can also be employed for data coding. The coding is done by switching a sequence of coding holograms on SLM1, and the decoding is accomplished by a Dammann vortex grating along with image processing. By using 16 various OAM states and four various radial indices, 6 bits multi-ring coding/decoding is accomplished. Additionally, a 64×64 gray image is transmitted through such 6 bits coding/decoding. The favorable experimental results indicate the good performance of data transmission. Moreover, we also evaluate the performance when facing atmosphere turbulence and find such turbulence will affect the decoding in the receiver, resulting in the increasing of BER. Due to the features that multi-ring vortices have, such as higher divergence angles, compared with single-ring vortices that carry identical OAM, the multi-ring coding/decoding scheme is more suitable for the scenario that asks for short-distance and large transmission capacity density. Hence, the proposed multi-ring optical-vortices-based high-dimensional data transmission will inspire potential applications in the future for short-distance and large-capacity optical data transmissions as optical interconnects and networks.

We acknowledge Miss Tonglu Wang of China Southern Industrial Academy for the helpful discussions when doing the experiment. This work was supported by the National Natural Science Foundation of China (NSFC) (No. 11834001), the National Postdoctoral Program for Innovative Talents of China (No. BX20190036), the China Postdoctoral Science Foundation (No. 2019M650015), and the Graduate Technological Innovation Project of Beijing Institute of Technology (No. 2018CX10020).

References

1. L. Allen, M. W. Beijersbergen, R. J. Spreeuw, and J. P. Woerdman, Phys. Rev. A **45**, 8185 (1992).
2. A. M. Yao and M. J. Padgett, Adv. Opt. Photon. **3**, 161 (2011).
3. J. Wang, J. Y. Yang, I. M. Fazal, N. Ahmed, Y. Yan, H. Huang, Y. Ren, Y. Yue, S. Dolinar, M. Tur, and A. E. Willner, Nat. Photon. **6**, 488 (2012).
4. A. E. Willner, H. Huang, Y. Yan, Y. Ren, N. Ahmed, G. Xie, C. Bao, L. Li, Y. Cao, Z. Zhao, J. Wang, M. P. J. Lavery, M. Tur, S. Ramachandran, A. F. Molisch, N. Ashrafi, and S. Ashrafi, Adv. Opt. Photon. **7**, 66 (2015).
5. S. Yu, Opt. Express **23**, 3075 (2015).
6. J. Wang, Chin. Opt. Lett. **15**, 030005 (2017).
7. T. Lei, M. Zhang, Y. Li, P. Jia, G. N. Liu, X. Xu, Z. Li, C. Min, J. Lin, C. Yu, H. Niu, and X. Yuan, Light: Sci. Appl. **4**, e257 (2015).
8. N. Zhao, X. Li, G. Li, and J. M. Kahn, Nat. Photon. **9**, 822 (2015).
9. M. Chen, K. Dholakia, and M. Mazilu, Sci. Rep. **6**, 22821 (2016).
10. A. Trichili, C. Rosales-Guzmán, A. Dudley, B. Ndagano, A. B. Salem, M. Zghalc, and A. Forbes, Sci. Rep. **6**, 27674 (2016).
11. M. P. J. Lavery, F. C. Speirits, S. M. Barnett, and M. J. Padgett, Science **341**, 537 (2013).
12. S. Fu, T. Wang, Z. Zhang, Y. Zhai, and C. Gao, Opt. Express **25**, 20098 (2017).
13. M. J. Padgett and R. Bowman, Nat. Photon. **5**, 343 (2011).
14. S. Fu, Y. Zhai, T. Wang, C. Yin, and C. Gao, Appl. Phys. Lett. **111**, 211101 (2017).
15. M. Malik, M. O'sullivan, B. Rodenburg, M. Mirhosseini, J. Leach, M. P. J. Lavery, M. J. Padgett, and R. W. Boyd, Opt. Express **20**, 13195 (2012).
16. A. Forbes, A. Dudley, and M. McLaren, Adv. Opt. Photon. **8**, 200 (2016).
17. S. Li and J. Wang, Opt. Express **25**, 21537 (2017).
18. Y. Zhang, F. S. Roux, M. McLaren, and A. Forbes, Phys. Rev. A **89**, 043820 (2014).
19. E. Karimi, D. Giovannini, E. Bolduc, N. Bent, F. M. Miatto, M. J. Padgett, and R. W. Boyd, Phys. Rev. A **89**, 013829 (2014).
20. M. Krenn, M. Huber, R. Fickler, R. Lapkiewicz, S. Ramelow, and A. Zeilinger, Proc. Natl. Acad. Sci. **111**, 6243 (2014).
21. S. Fu and C. Gao, Photon. Res. **4**, B1 (2016).
22. Y. Ren, H. Huang, G. Xie, N. Ahmed, Y. Yan, B. I. Erkmen, N. Chandrasekaran, M. P. J. Lavery, N. K. Steinhoff, M. Tur, S. Dolinar, M. Neifeld, M. J. Padgett, R. W. Boyd, J. H. Shapiro, and A. E. Willner, Opt. Lett. **38**, 4062 (2013).
23. Y. Ohtake, T. Ando, N. Fukuchi, N. Matsumoto, H. Ito, and T. Hara, Opt. Lett. **32**, 1411 (2007).
24. B. Sephton, A. Dudley, and A. Forbes, Appl. Opt. **55**, 7830 (2016).
25. M. Rafayelyan and E. Brasselet, Opt. Lett. **42**, 1966 (2017).
26. N. Zhang, X. C. Yuan, and R. E. Burge, Opt. Lett. **35**, 3495 (2010).
27. S. Fu, T. Wang, S. Zhang, and C. Gao, Appl. Opt. **55**, 1514 (2016).
28. D. L. Fried, J. Opt. Soc. Am. **55**, 1427 (1965).
29. R. G. Lane, A. Glindemann, and J. C. Dainty, Waves Random Media **2**, 209 (2006).
30. Y. Ren, G. Xie, H. Huang, C. Bao, Y. Yan, N. Ahmed, M. P. J. Lavery, B. I. Erkmen, S. Dolinar, M. Tur, M. A. Neifeld, M. J. Padgett, R. W. Boyd, J. H. Shapiro, and A. E. Willner, Opt. Lett. **39**, 2845 (2014).
31. S. Li and J. Wang, Opt. Lett. **41**, 1482 (2016).
32. S. Fu, S. Zhang, T. Wang, and C. Gao, Opt. Lett. **41**, 3185 (2016).
33. S. Fu, T. Wang, S. Zhang, Z. Zhang, Y. Zhai, and C. Gao, Photon. Res. **5**, 251 (2017).